Environment Protection Engineering

Vol. 47 2021 No. 2

DOI:10.37190/epe210203

KAVIYA PIRIYAH SUNDAR (ORCID: 0000-0003-2728-2434)[1]

SELLAPA KANMANI[1]

STUDIES ON THE DEVELOPMENT OF A NOVEL UV-LED STRIP PHOTOCATALYTIC REACTOR AND PERFORMANCE ON DYE REMOVAL

The challenges of photocatalytic reactor design are addressed in the present study, focusing on developing novel reactor configurations for uniform light intensity, high photon, and mass transfer efficiencies. This work developed a scalable compact UV-LED strip photocatalytic reactor comprising of a quartz tube placed inside the aluminum shell. The light source, i.e., 300 LEDs (λ_{max} = 365 nm) circumferentially disposed in the inner walls of shell and reactor's performance was evaluated for 3.12×10^{-5} mol/dm^3 methylene blue for 80% dye removal in 60 min for optimized conditions. Hydrodynamic cavities were induced by the constricted geometry and inlet pressure, which may increase the dye removal. Actinometry was performed and photonic efficiency was evaluated to be 25%, which proves that the present reactor is an efficient configuration allowing maximum dye degradation.

1. INTRODUCTION

Advanced oxidation processes are advantageous over other physicochemical methods such as flocculation, reverse osmosis, and adsorption because these methods are non-destructive and only transfers the pollutant from one form to the other form giving rise to secondary pollution [1]. Recently heterogeneous photocatalysis studies [2] have been focused on the degradation of a large number of recalcitrant organics. Heterogeneous photocatalysis is defined as a light-induced oxidation process in the presence of a solid-phase catalyst for the removal of fluid phase pollutants. Heterogeneity of process makes the photocatalytic reactor design challenging.

There were various photocatalytic reactors designed so far. In the early nineties, solar reactors (developed by Plataforma Solar de Almeria (PSA), Spain and National

[1]Centre for Environmental Studies, Anna University, Chennai-600 025, Tamil Nadu, India, corresponding author K.P. Sundar, email address: kaviya1305@gmail.com

Renewable Energy Laboratory (NREL), California (US)) including parabolic trough reactor (PTR), thin-film fixed-bed reactor (TFFBR), compound parabolic collecting reactor (CPCR), double skin sheet reactor (DSSR) were designed [3]. Due to the slower reaction kinetics of solar photocatalytic reactors, designs were based on artificial light sources. Classical annular reactor (CAR) was the basic reactor, where the lamp was located at the center and the reactant was outside as a shell. The main disadvantage of the CAR was the absence of agitation, difficult catalyst recovery, and uneven light illumination through the reaction medium. Further to ease the catalyst separation process, various immobilized reactors such as fluidized bed reactor (FBR), tube light reactor (TLR), multi-tube reactor (MTR), spinning disc reactors (SDR) were designed [4]. The major issues in these types of immobilized reactors were the uneven light distribution inside the reactor. For channelizing the light photons, TiO_2 coated optical fiber photoreactors (OFR) were developed, where backlighting was a major drawback [5].

The conventional lamps were heating the system, also containing toxic substances, so reactors were designed by using energy-efficient light-emitting devices (LEDs). LEDs have numerous advantages including lower energy consumption, longer lifetime, high compactness and flexibility in design, and faster switching. Later the focus of the design was to increase the specific surface area of the reaction medium under illumination. Firstly, it was done by incorporation of micro-channels in reactors such as capillary array photocatalytic reactor (CAPR) and micro-reactors and secondly by the use of nano-sized catalysts. To ease the separation of slurry nano-catalyst systems, membrane reactors were designed. Micro-reactors are advantageous because of their large surface-to-volume ratios enhancing the rate of reaction, but throughput was the major issue [6]. Then to mimic the micro-pocket environment in reactors, immobilized packed bed reactors (PBR) were designed. The major drawback of PBR could be the scattering and loss of photons when they hit the packed media which is used for catalyst immobilization. Therefore it is very important to design a reactor with uniform light intensity throughout the reaction medium [7].

Concerning catalyst, TiO_2 is an effective photocatalyst for air, water, and wastewater treatment for its excellent properties of high chemical stability, non-toxicity, high reactivity, and cost-effectiveness [8]. But one of the major limitations of TiO_2 is the faster electron-hole recombination. On the other hand, graphene has attracted more research publications since its discovery in 2004 due to its superior electrical and chemical properties [9, 10]. Graphene is a single sheet layer of graphite that has a large surface area (ca. 2600 m^2/g) with enhanced reactivity. Also, graphene decorated with various metal nanoparticles and TiO_2 nanoparticles has been evaluated for degradation of dyes in many papers [11].

Various works focused on LED-based reactors, but the present one focuses on overcoming the challenges faced in designing a photocatalytic reactor. The major challenges faced in the LED-based photocatalytic reactors (packed bed reactors and micro-reac-

tors) are uniform light distribution and high throughput. Uniform light irradiation enhances the delivery of the light photons to photocatalyst active sites. The present work focused on the design and development of a scalable compact UV-LED strip photocatalytic reactor offering uniform light distribution achieved by circumferential disposal of light sources, i.e., LEDs. This reactor configuration was optimized for process parameters for methylene blue (MB) dye degradation using graphene as a catalyst. Ferri-oxalate actinometry was performed to find the photon flux (moles of incident photons/seconds) and correlated with the moles of MB dye decolorized to find the photonic efficiency (achieved was 25%). Similar studies have been done by Alrobayi et al. [12] for the evaluation of photonic efficiency of 8% for Maxilon blue dye degradation in the presence of synthesized TiO_2 nanoparticles and Jamali et al. [13] for the evaluation of photonic efficiency of batch LED reactor to be around 0.86%. Therefore the present reactor is efficient in terms of high compactness, uniform irradiation, high throughput, and easy scalability, which are the drawbacks of existing LED-based reactors.

2. EXPERIMENTAL

Reactor design. The reactor consisted of an outer cylindrical shell made up of aluminum (170 mm long and 145 mm in diameter) and there are attachable enclosure caps at both sides consisting of an aperture of 35 mm in diameter at its center for the quartz tube to pass through.

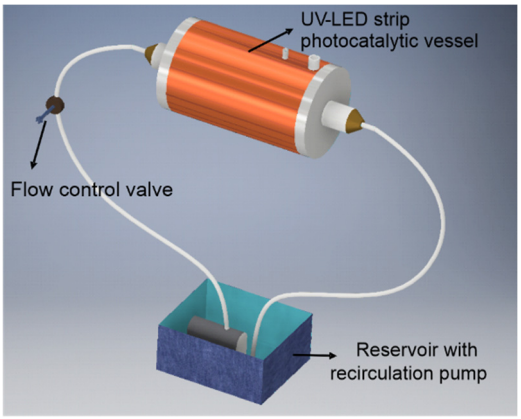

Fig. 1. UV-LED photocatalytic reactor

The quartz tube (capacity 170 cm^3) 240 mm long and 30 mm in diameter passes through the outer shell where mid 170 mm is within it and the rest supported by the apertures of caps outside it. The thickness of both the outer cylindrical shell and quartz tube was around 2 mm. A 5 m long UVA LED strip consisting of 300 light-emitting

diodes (LEDs) emitting radiation of 365 nm wavelength, was positioned in a circumferential manner inside the outer shell. The 12 V DC 24 W 2 A UVA LED strip thickness was 0.2 mm and width – 8 mm, which made the reactor a compact design. The distance between the dye solution and the LED strip is 5 cm. The one end (inlet) of the quartz tube was connected with a pipe which in turn is connected to a recirculating pump of 230 V AC 50 Hz 18 W. There is an outer cooling jacket, located around the aluminum shell for temperature maintenance (Figs. 1, 2).

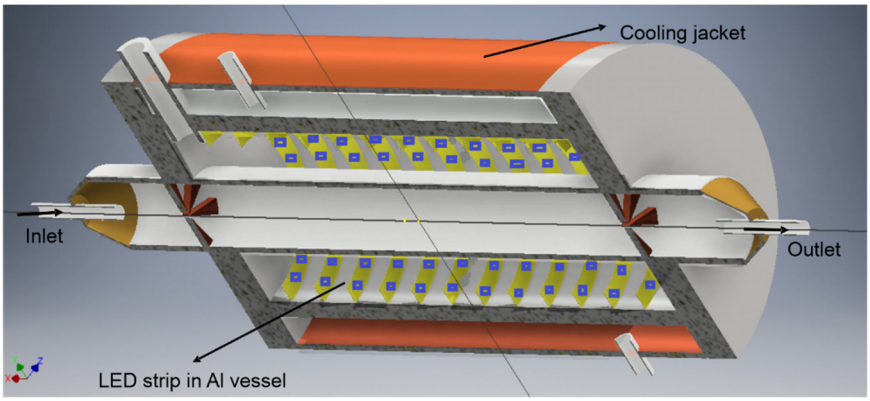

Fig. 2. Internal configuration of the reactor

Quantity of LEDs. Estimation. The UV-LED strip photocatalytic reactor was designed to simulate the UVA portion of solar irradiation inside the reactor vessel. The Sun's total light intensity at ground level is around 1050 W/m^2 [14]. The calculation was done for estimating the number of LEDs required for simulating the same intensity to that of UVA portion (3%) of sunlight intensity (ca. 30 W/m^2).

The effective area for light exposure (internal area of quartz tube) was 0.01 m^2

$$\Phi_V = E_v A \tag{1}$$

where Φ_V is the luminous flux (lm), E_v is illuminance (lux) and A is the surface area irradiated inside the reactor (m^2). The unhidden Sun provides an illumination of up to 100 klux on the Earth's surface. Lumens required for this specific reactor: 10^5 lux × 0.01 m^2 = 1000 lm. Watts required: 1000/42 = 23.8 W = ca. 24 W (LED offers 42 lm/W). Watt per LED piece = 0.08 W. Number of LEDs required: 24/0.08 = 300. Hence 5 m strip containing 300 LEDs was circumferentially wrapped inside the walls of the reactor. The UVA light meter (UV-340A Lutron) was used to measure the light intensity inside the reactor as 27–30 W/m^2 which is comparable with the UVA portion of solar radiation (ca. 3%).

Graphene preparation. Graphene powder was prepared as per modified Hummer's method, where 1 g of graphite and 0.5 g of $NaNO_3$ were mixed with 23 cm^3 of concentrated H_2SO_4 under continuous stirring. After an hour, 3 g of $KMnO_4$ was added slowly

to the mixture while keeping the temperature around 20 °C. After 12 h of mixing, 500 cm^3 of water was added under vigorous stirring. Then 5 cm^3 of 30% H_2O_2 was added and the resulting mixture was filtered, washed with HCl and H_2O_2, and dried to obtain graphene nanopowder [15].

Material characterization. The wavelength of procured UVA-LED radiation was checked for peak intensity count. A wavelength–intensity graph was obtained using a fibre optics spectrometer CCS100M, where the maximum intensity was observed at 370 nm for UVA LEDs (Fig. 3).

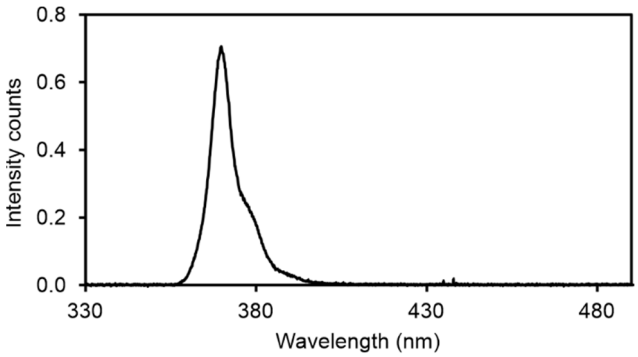

Fig. 3. LED wavelength characterisation

The photocatalyst was characterized for average particle size by dynamic light scattering (DLS) using a Malvern zetasizer. The average particle size was 458 nm (Fig. 4).

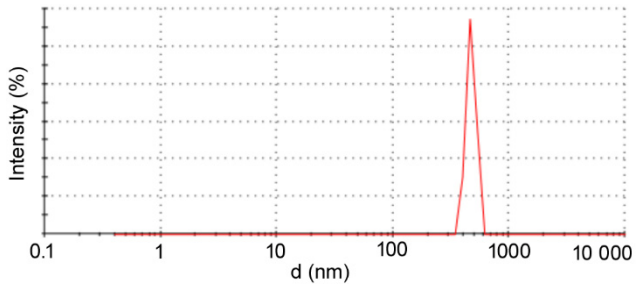

Fig. 4. Size distribution by intensity

The morphology was analyzed by scanning electron microscopy (SEM). The SEM image was recorded using Carl Zeiss Evo 18 microscope (accelerating voltage 15 kV). The sample powder was spread on a carbon-coated sample mount and coated with gold to prevent surface charging effects. Graphene shows a flaky layer-like structure which reveals the oxidation of graphite [16] (Fig. 5).

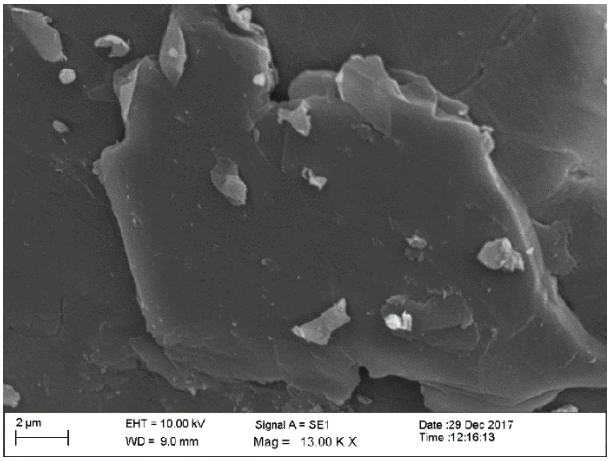

Fig. 5. SEM image of graphene

The elemental composition was detected using energy dispersive spectroscopy (EDS) (Fig. 6). The photocatalyst graphene was rich in carbon (C), oxygen (O), rather than any other elements. A low concentration of Au/Pd alloy was used for sputtering, therefore minimal concentration was found. Neglecting the Au/Pd, the contents of C and O was 81.81% and 18.18%, respectively, which indicates that the photocatalyst was synthesized successfully.

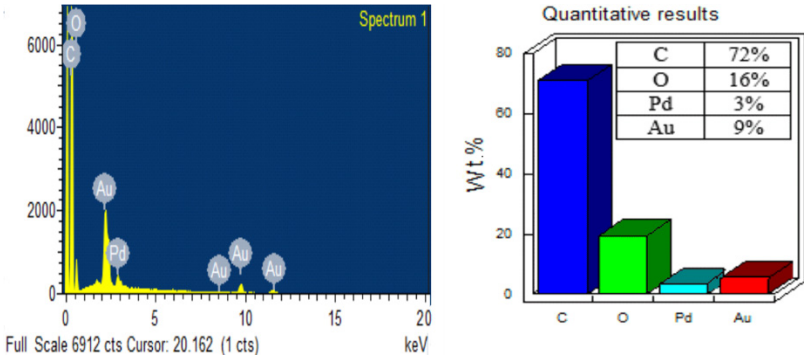

Fig. 6. Elemental composition of photocatalyst

Bang gap was calculated using UV-Vis spectroscopic analysis (JASCO V-650) to measure diffuse reflectance. The reflectance data was converted to absorption coefficient using the Kubelka–Munk radiative transfer model as shown in Fig. 7. The bandgap energy (*BGE*, eV) of graphene was calculated using the following formula:

$$BGE = \frac{1240}{\lambda} \tag{2}$$

The BGE of graphene was 3.28 eV (378.4 nm). The band gap energy obtained is comparable with that calculated elsewhere [17].

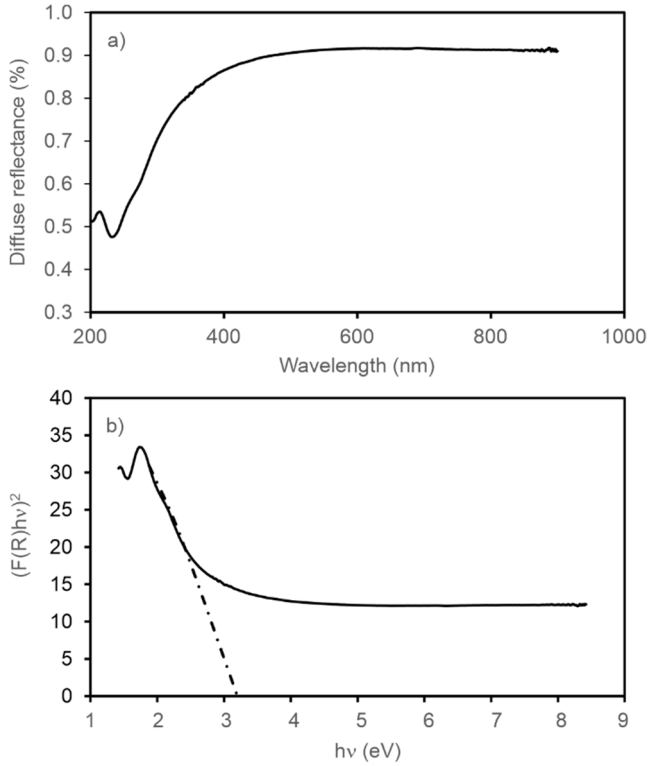

Fig. 7. Measured diffuse reflectance for graphene (a) and band-gap wavelength (3.28 eV) (b) obtained from linear extrapolations using the Kubelka–Munk radiative transfer model

Experimental procedure. The performance of the UV-LED strip photocatalytic reactor was evaluated under the batch recirculation process. A methylene blue (MB) dye solution (3.12×10^{-5} mol/dm^3) was first stirred under dark for 30 min to attain adsorption–desorption equilibrium between the photocatalyst and dye before the irradiation. The initial reading was recorded as zero-minute reading. After the start of irradiation, A 5 cm^3 sample was withdrawn every 15 min during the experiment. The sample was centrifuged at 10000 rpm (REMI R-24) for 5 min to separate the graphene photocatalyst. Then the supernatant was analyzed by UV-visible spectrophotometer at 665 nm. The effect of recirculation rate (350–2000 cm^3/min) was investigated by controlling the inlet valve of UV-LED reactor and optimized. For the evaluation of optimized pH value in a wide pH range (4–12), 1 mol/dm^3 HCl and 1 mol/dm^3 NaOH solutions were used for

adjusting the pH value of the dye solution. The catalyst dosage was varied from 0.02 to 0.1 g/dm^3 and the light intensity of 300 UVA LEDs (27 W/m^2) and 300 visible white LEDs (9140 lux) were investigated and optimized. A UV-340A Lutron light meter and TES 1332A lux meter were used to measure the intensities of UVA and visible light. All the experiments were conducted for the irradiation time of 60 min.

Ferrioxalate actinometry. Actinometry procedure was followed according to the Hatchard–Parker method [18]. First, the volume of 3 cm^3 (V_1) of 0.006 mol/dm^3 ferrioxalate solution (2.947 g of the crystals dissolved in 100 cm^3 of 0.5 M H_2SO_4 and diluted with distilled water to 1 dm^3) was irradiated for 60 min. Then, 1 cm^3 (V_2) of the solution irradiated for 60 min was placed in a 10 cm^3 (V_3) volumetric flask containing a mixture of 4 cm^3 0.1% 1.10-phenanthroline solution which is stored in dark and 0.5 cm^3 buffer (stock solution: 82 g $NaC_2H_5CO_2$, 10 cm^3 of concentrated H_2SO_4, diluted to 1 dm^3 with distilled water) which was then diluted to the mark with distilled water. A reference (not irradiated) was prepared in the same way. Both solutions were kept in the dark until full-color development was achieved and the absorbance difference between the two samples was measured at 510 nm (1 cm optical pathlength (l), ε_{510} = 11 100 dm^3/(mol·cm)). It is to be noted that A_{510} should be within the range of 0.4–1.8. In our experiment, the color difference was observed as shown in Fig. 3 and the absorbance difference (ΔA) of 1.051 at 510 nm was noted (Fig. 8). N_p was calculated using the below formula:

$$N_p = \frac{\Delta A V_1 V_3}{\varphi_\lambda \varepsilon_{510} V_2 l t} \times 10^{-3} \tag{3}$$

where N_p is incident photon flux (mol/s), V_1, V_2, V_3 – volumes of solutions (cm^3), l – the optical pathlength (cm), t – the reaction time (s), ε_{510} is the molar absorptivity (dm^3/(mol·cm)) and φ_λ – the quantum yield of known chemical actinometer. φ_λ is 1.2–1.26 for the wavelength range of 254–366 nm.

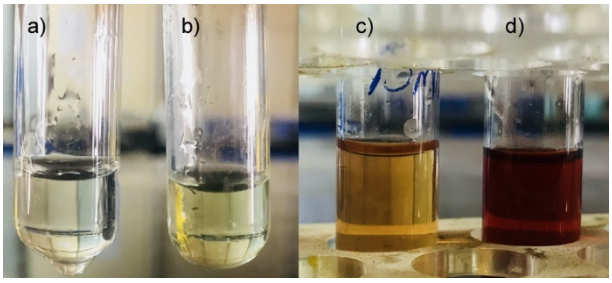

Fig. 8. Samples: a) 0.06 mol/dm^3 ferrioxalate solution irradiated for 60 min, b) reference 0.06 mol/dm^3 ferrioxalate solution, c) reference after addition of 0.1% 1,10-phenanthroline (A at 510 nm – 0.772), d) after addition of 0.1% 1,10-phenanthroline (A at 510 nm – 1.823) irradiated for 60 min

$$R = \frac{V\Delta C}{1000Mt} \tag{4}$$

where R is the reaction rate (mol/s), ΔC is the change in concentration of dye (mg/dm^3), V – the volume of a sample treated (cm^3), M – molecular weight (319.85 g/mol), t – time (s). The photonic yield (ξ_λ) is the ratio between reaction rate and photon flux incident for the time of 60 min [18, 19]. R (for 80% decolorization) is 6.95×10^{-9} mol/s and N_p was 278.35×10^{-10} mol/s. The ξ_λ was calculated as 0.25.

3. RESULTS AND DISCUSSIONS

The performance of the photocatalytic reactor was evaluated for MB dye removal (3.12×10^{-5} mol/dm^3) by graphene under UV-LED irradiation. The results demonstrated that 80% of MB dye was removed under this configuration of UV-LEDs inside the reactor in the presence of graphene photocatalyst, whereas in the absence of a light source 30% of MB was decolorized after 2 h (Fig. 9). The results of adsorption measurements indicate that graphene acts as a good adsorbent of MB dye [20].

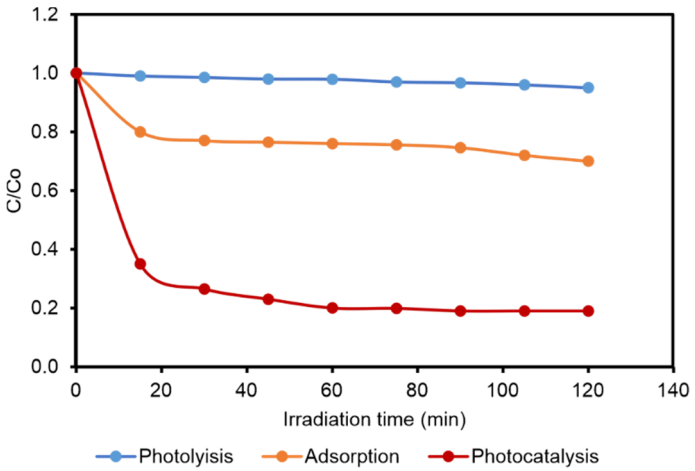

Fig. 9. Relative dye concentration (C/C_0) in dependence of the irradiation time for photolysis, adsorption and photocatalysis (graphene dose 0.05 g/dm^3, initial pH 11, recirculation rate 700 cm^3/min and 27 W/m^2 UVA light intensity)

3.1. EFFECT OF RECIRCULATION RATE

To find the optimum rate of recirculation for the working of UV-LED strip photocatalytic reactor for maximum MB removal, the recirculation rate was varied from 350 to 2000 cm^3/min. The concentration of MB in solution was 3.12×10^{-5} mol/dm^3 for all

the experiments. Figure 10 shows the effect of recirculation rate on decolorization of MB dye solution which increased upon increasing recirculation rate until a particular point (700 cm^3/min), then decreased with further increase. The highest dye removal of 23% was achieved at 700 cm^3/min in the presence of catalyst dosage of 0.02 g/dm^3 under UV-LED irradiation.

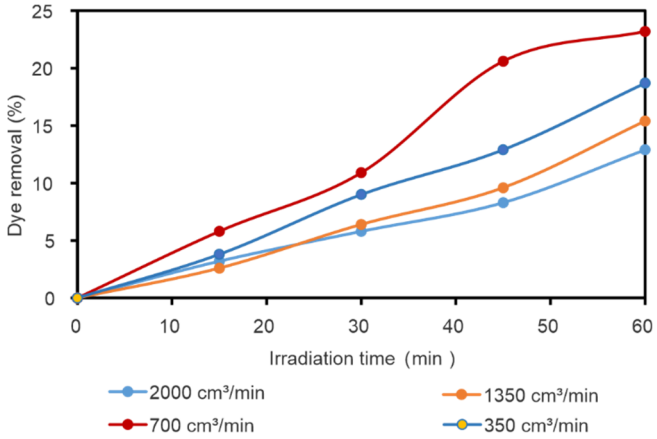

Fig. 10. Time dependences of dye removal for various recirculation rates (graphene dosage: 0.02 g/dm^3, initial pH 6 and 27 W/m^2 UVA light intensity)

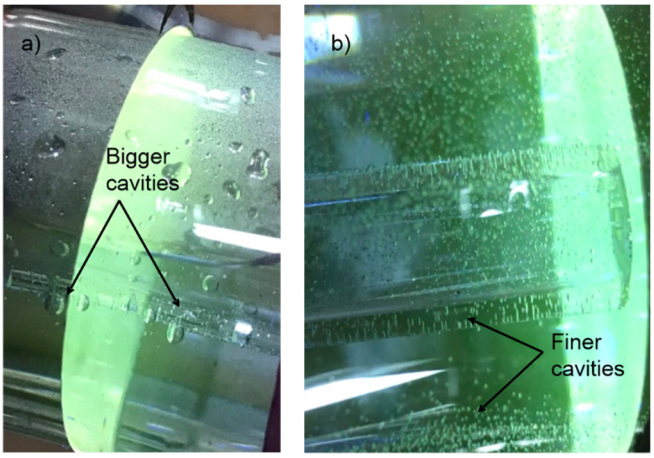

Fig. 11. Big cavities at the recirculation rate of 2000 cm^3/min (a), and finer cavities at the recirculation rate of 350 cm^3/min (b)

In this case of batch recirculation, there should be two aspects considered: residence time per pass in the quartz tube and exposure time of the entire volume of dye solution. At the highest rate of recirculation (2000 cm^3/min), the residence time inside the reactor is the

shortest, but the overall exposure of the solution to UV irradiation was high, hence dye removal was the lowest. However, at the lowermost rate of recirculation (350 cm^3/min), the residence time (per pass) in the reactor was the longest, but the exposure time of the entire volume of solution was the shortest, hence the efficiency of dye removal was comparable with that obtained at the highest rate of recirculation. Therefore, at the intermittent rate of recirculation (700 cm^3/min) there is a balance between the residence time per pass and overall exposure time to attain maximum efficiency of dye removal. Sraw et al. [21] studied the similar pattern for effect on recirculation rate in the pesticide water degradation on fixed bed recirculation type photocatalytic reactor with TiO_2 immobilized clay beads, where the optimum flow rate was 400 cm^3/min (78% degradation) when varied from 100 to 800 cm^3/min.

There were numerous fine cavities in the quartz tube which were formed at the lowest rate of recirculation. However, beyond the optimum rate of recirculation, larger cavities of fewer numbers were observed (Fig. 11).

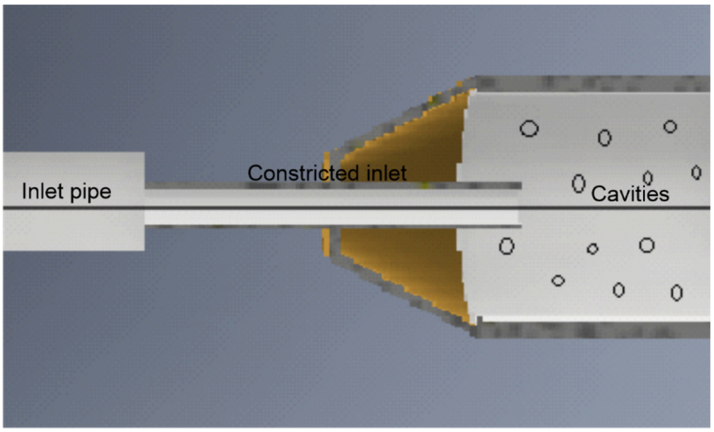

Fig. 12. Hydrodynamic cavitation using constricted geometry

The reactor employs hydrodynamic cavitation, where cavities were formed by the constricted tube provided in the reactor inlet (Fig. 12). The pressure at the narrow cross-section of the inlet (constriction) falls below the vapor pressure of the methylene blue solution and when the pressure recovers in the quartz tube, there is a generation of numerous cavities that subsequently collapse creating hot spots, releasing highly reactive free radicals. The collapse of bubbles may induce transient temperature of the order of 10 000 K and pressures of about 100 MPa. Under such extreme conditions, water molecules dissociate into $OH^{\bullet}$ and $H^{\bullet}$ radicals. These $OH^{\bullet}$ radicals then diffuse into the bulk liquid medium where they degrade the dye molecules. This hydrodynamic cavitation further enhances dye degradation by the increase in mass transport due to the collapse of cavities [22].

3.2. EFFECT OF CATALYST DOSAGE

Catalyst dosage in the photocatalytic process is a particularly important parameter (Fig. 13). The dye removal from MB solution increased with the increase in graphene dose from 0.02 to 0.05 g/dm^3 and then further increase in catalyst dosage decreased the dye removal. This may be due to the increase in active sites with the addition of catalyst particles. Later there is a predominant particle aggregation, shielding the photocatalyst active sites. Another reason may be due to the increase in recombination centers at a higher dosage of photocatalyst particles. Hence, an optimum catalyst dosage is to be used to maximize photonic efficiency and avoid excess usage. Similar studies were made by Bora et al. [23] for the study of operational parameters including type and dosage of photocatalyst, pH, light intensity, dopant, pollutant type, concentration, etc. Also, Mia et al. [24] performed experiments on TiO_2-assisted photodegradation of the Victoria Blue R (VBR) where the optimum catalyst dosage was 0.5 g/dm^3 for the solution containing 50 mg/dm^3 of VBR dye, where the intermediate catalyst dosage proved to be efficient.

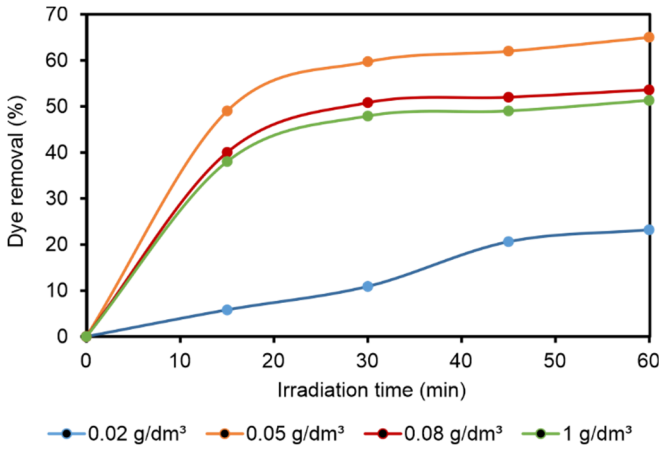

Fig. 13. The effect of graphene dosage on dye removal
(recirculation rate 700 cm^3/min, initial pH 6 and 27 W/m^2 UVA light intensity)

3.3. EFFECT OF INITIAL PH

The initial pH is a major factor influencing the rate of photocatalytic degradation. The study of absorption spectrum (Fig. 14) shows that the changes in the pH values significantly change the absorbance of MB solution and affect the rate of photocatalysis. The initial pH of MB dye (3.12×10^{-5} mol/dm^3) was 6. The decolorization of MB solution achieved amounted to 65%. When the initial pH was lowered from 6 to 4, the MB removal decreased to 58%. On the other hand, when pH was increased from 6 to 11, the

photocatalytic activity increased gradually from 65% to 80%. Further increasing pH to 12, decreased the color removal efficiency to 74% (Fig. 15).

This may be since MB is a cationic dye and in alkaline solutions, the surface area of photocatalyst may possess a negative charge due to the adsorption of OH^- groups onto the catalytic surface. In turn, this enhances the attraction between catalyst particles and MB dye leading to enhanced reactivity. The results observed were similar to those by Tayade et al. [25], which indicated that the initial pH 8.84 was optimum for maximum MB removal from water solution (6.25×10^{-5} mol/dm^3) using P-25 Degussa TiO_2 under UV-LED irradiation.

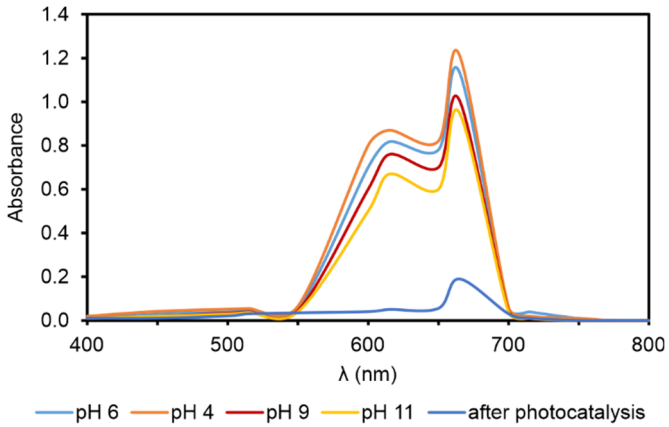

Fig. 14. Absorption spectrum of MB solution at varying initial pH and after photocatalysis (optimized conditions: initial pH 11, graphene dosage 0.05 g/dm^3, recirculation rate 700 cm^3/min and 27 W/m^2 UVA light intensity)

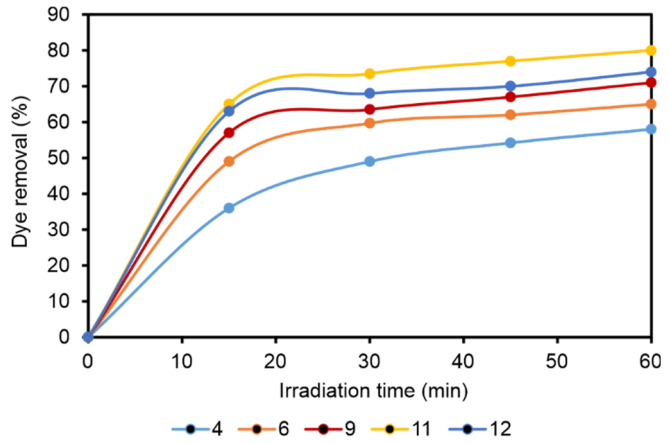

Fig. 15. The effect of initial pH on dye removal (graphene dosage 0.05 g/dm^3, recirculation rate 700 cm^3/min and 27 W/m^2 UVA light intensity)

3.4. EFFECT OF LIGHT INTENSITY

In the presence of UVA-LED irradiation, the maximum removal of 80% was achieved (Fig. 16) due to the higher energy of photons emitted by UVA LED source and more effective electron-hole formation, where the rate of reaction is linearly dependent on the light intensity at lower levels of irradiance (up to 200 W/m^2) [4]. Afsoon et al. [13] studied the increase in degradation with the increase in irradiance on batch LED reactor for phenol degradation, where the drive current was adjusted to increase the irradiance up to 9.055W/m^2.

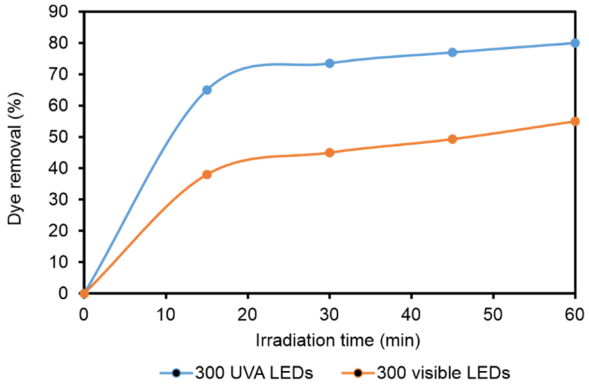

Fig. 16. The effect of light intensity on dye removal
(graphene dose 0.05 g/dm^3, recirculation rate 700 cm^3/min and initial pH 11)

3.5. XRD ANALYSIS BEFORE AND AFTER PHOTOCATALYSIS

Figure 17 illustrates the XRD pattern for graphene photocatalyst before and after the reaction.

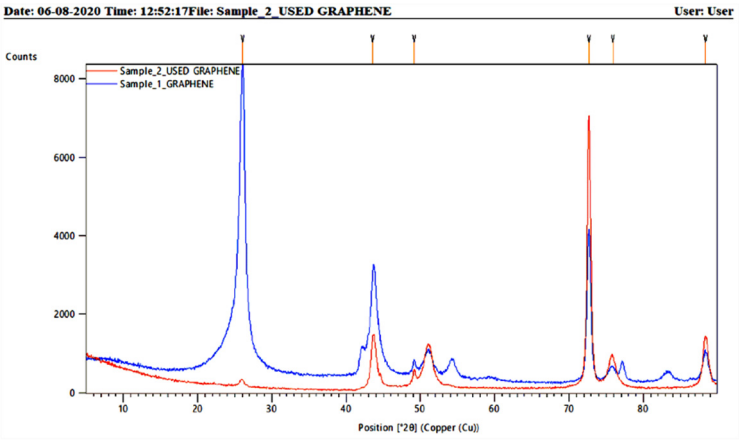

Fig. 17. XRD patterns of graphene before and after reaction

The main characteristic peak of graphene photocatalyst was at 26.17°, which could be correlated with previous works [26]. The intensity of the diffraction peak decreased after photocatalytic reaction implying that there is a decrease in crystallinity. Also, the full-width half maximum decreased after reaction due to an increase in crystallite size from 14 to 19 nm. The increase in crystallite size may be due to occluded degradation by-products onto the photocatalyst surface. For further reuse of the photocatalyst, a regeneration procedure is to be carried out by suspending the photocatalyst in water overnight and exposing them to UVA irradiation up to 16 h [27].

4. CONCLUSIONS

This present work overcomes the challenges faced by the design of photocatalytic reactors. The two main issues addressed are (i) uniform light irradiation, (ii) throughput wherein the two factors determine the performance and scalability of LED-based photocatalytic reactors. The present invention uses slender UV-LED strips by providing a compact photocatalytic reactor where uniformity in the light distribution is achieved by disposing UV LEDs in a circumferential direction of reactor walls. Further hydrodynamic cavities were induced by constricted geometry and inlet pressure. From the experiments, it was observed that 80% removal was achieved for methylene blue dye solution at optimum conditions. Photonic efficiency of 25% proves that the photon capture is maximum in the present reactor configuration. Although the reactor was evaluated for degradation of synthetic dye, this reactor could also be applied for disinfection, water splitting, emerging contaminants degradation, etc. Future research could focus on the performance evaluation of this reactor configuration in bench-scale and pilot-scale levels for other emerging contaminants.

REFERENCES

[1] BELVER C., BELLOD R., FUERTE A., FERNANDEZ-GARCIA M., *Nitrogen-containing TiO_2 photocatalysts: Part 1. Synthesis and solid characterization*, Appl. Cat. B: Environ., 2006, 65, 301–308. DOI: 10.1016/j.apcatb.2006.02.007.

[2] SERPONE N., *Brief introductory remarks on heterogeneous photocatalysis*, Solar En. Mater. Solar Cells, 1995, 38 369–379. DOI: 10.1016/0927-0248(94)00230-4.

[3] KANMANI S., THANASEKARAN K., BECK D., *Performance studies on novel solar photocatalytic reactors for decolourization of textile dyeing wastewaters*, Indian J. Chem. Techn., 2003, 10, 638–643. DOI: http://nopr.niscair.res.in/bitstream/123456789/22806/1/IJCT%2010(6)%20638-643.pdf

[4] LEBLEBICI E., STEFANIDIS G.D., GERVEN T.V., *Comparison of photocatalytic space-time yields of 12 reactor designs for waste water treatment*, Chem. Eng. Proc., 2015, 97, 106–111. DOI: 10.1016/j.cep.2015.09.009.

[5] LIN H., VALSARAJ K.T., *Development of an optical fiber monolith reactor for photocatalytic wastewater treatment*, J. Appl. Electrochem., 2005, 35, 699–708. DOI: https://link.springer.com/article/10.1007/s10800-005-1364-x.

[6] GORGES R., KREISEL G., *Photocatalysis in microreactors*, J. Photochem. Photobiol. A: Chemistry, 2004, 167, 95-99. DOI: 10.1016/j.jphotochem.2004.04.004.
[7] SUNDAR K.P., KANMANI S., *Progression of photocatalytic reactors and it's comparison. A review*, Chem. Eng. Res. Design, 2020, 154, 135–150. DOI: 10.1016/j.cherd.2019.11.035.
[8] FUJISHIMA A., RAO T.N., TRYK D.A., *Titanium dioxide photocatalysis*, J. Photochem. Photobiol. C: Photochem. Rev., 2000, 1, 1–21. DOI: 10.1016/S1389-5567(00)00002-2.
[9] LIANG H.F., SMITH C.T.G., MILLS C.A., SILVA S.R.P., *The band structure of graphene oxide examined using photoluminescence spectroscopy*, J. Mater. Chem. C, 2015, 3, 12484. DOI: 10.1039/C5TC00307E.
[10] SHEN Y., YENG S., ZHOU P., SUN Q., WANG P., WAN L., LI J., CHEN L., WANG X., DING S., ZHANG D.W., *Evolution of band gap and optical properties of graphene oxide with controllable reduction level*, Carbon, 2013, 62, 157–164. DOI: 10.1016/j.carbon.2013.06.007.
[11] LI X., YU J., WAGEH S., AL-GHAMDI A.A., XIE J., *Graphene in photocatalysis: A review*, 2016, 12, 6640–6696. DOI: 10.1002/smll.201600382.
[12] ALROBAYI E.M., ALGUBILI A.M., ALJEBOREE A.M., ALKAIM A.F., HUSSEIN F.H., *Investigation of photocatalytic removal and photonic efficiency of maxilon blue dye GRL in the presence of TiO_2 nanoparticle*s, Part. Sci. Techn., 2015, 35, 1–7. DOI: 10.1080/02726351.2015.1120836.
[13] JAMALI A., VANRAES R., HANSELAER P., GERVEN T.V., *A batch LED reactor for the photocatalytic degradation of phenol*, Chem. Eng. Proc., 2013, 71, 43–50. DOI: 10.1016/J.CEP.2013.03.010.
[14] MIASIK D.P., RABCZAK S., *Impact of solar radiation change on the collector efficiency*, J. Ecol. Eng., 2017, 18, 268–272. DOI: 10.12911/22998993/67106.
[15] SHAHRIARY L., ATHAWALE A., *Graphene oxide synthesized by using modified hummers approach*, Int. J. Ren. En. Environ. Eng., 2014, 2, 58–63.
[16] ULLAH K., YE S., ZHU L., JO S.B., JANG W.K., CHO K.Y., OH W.C., *Noble metal doped graphene nanocomposites and its study of photocatalytic hydrogen evolution*, Solid State Sci., 2014, 31, 91–98. DOI: 10.1016/j.solidstatesciences.2014.03.006.
[17] HATCHARD C.G., PARKER C.A., *A new sensitive chemical actinometer. II. Potassium ferrioxalate as a standard chemical actinometer*, Proc. Royal Society A, London 1956, A235, 518–536. DOI: 10.1098/rspa. 1956.0102.
[18] KUHN H.J., BRASLAVSKY S.E., SCHMIDT R., *Chemical actinometry (IUPAC Technical Report)*, Pure Appl. Chem., 2004, 76 (12), 2105–2146. DOI: 10.1351/pac200476122105.
[19] XIONG Z., ZHANG L.L., MA J., ZHAO X.S., *Photocatalytic degradation of dyes over graphene–gold nanocomposites under visible light irradiation*, Chem. Com., 2010, 46, 6099–6101. DOI: 10.1039 /c0cc01259a.
[20] SRAW A., KAUR T., PANDEY Y., SOBTI A., WANCHOO R.K., TOOR A.P., *Fixed bed recirculation type photocatalytic reactor with TiO_2 immobilized clay beads for the degradation of pesticide polluted water*, J. Environ. Chem. Eng., 2018, 6, 7035–7043. DOI: 10.1016/j.jece.2018.10.062.
[21] SAHARAN V.K., BADVE M.P., PANDIT A.B., *Degradation of Reactive Red 120 dye using hydrodynamic cavitation*, Chem. Eng. J., 2011, 178, 100–107. DOI: 10.1016/j.cej.2011.10.018.
[22] BORA L.V., MEWADA R.K., *Visible/solar light active photocatalysts for organic effluent treatment: Fundamentals, mechanisms and parametric review*, Ren. Sust. En. Rev., 2017, 76, 1393–1421. DOI: 10.1016/j.rser.2017.01.130.
[23] MIA F.D, LU C.S., WU C.W., HUANG C.H., CHEN J.Y., CHEN C.C., *Mechanisms of photocatalytic degradation of Victoria Blue R using nano-TiO_2, separation and purification technology*, 2008, 62, 423–436. DOI: 10.1016/j.seppur.2008.02.006.
[24] TAYADE R., NATARAJAN T.S., BAJAJ H.C., *Photocatalytic degradation of methylene blue dye using ultra-violet light emitting diodes*, Ind. Eng. Chem. Res., 2009, 48, 10262–1026. DOI: 10.1021/ie9012437.

[25] SAMPATH S., KANMANI S., *Visible-light-driven photocatalysts for hydrogen production by water splitting*, En. Sources, Part A: Rec., Util., Environ. Effects, 2020, 42 (6), 719–729. DOI: 10.1080 /15567036.2019.1602194.

[26] LINLEY S., LIU Y.Y., PTACEK C.J., BLOWES D.W., GU F.X., *Recyclable graphene oxide-supported titanium dioxide photocatalysts with tunable properties*, Am. Chem. Soc. Appl. Mater. Interf., 2014, 6 (7), 4658 –4668. DOI: 10.1021/am4039272.